Journal of Pharmaceutical and Biomedical Analysis 51 (2010) 30–38

Contents lists available at ScienceDirect

Journal of Pharmaceutical and Biomedical Analysis

journal homepage: www.elsevier.com/locate/jpba

Raman microscopic evaluation of technology dependent structural differences in tablets containing imipramine model drug

Balázs Vajna [a,*], István Farkas [a], András Szabó [a], Zsolt Zsigmond [b], György Marosi [a]

[a] Department of Organic Chemistry and Technology, Budapest University of Technology and Economics, Budafoki út 8, H-1111 Budapest, Hungary
[b] EGIS Pharmaceuticals Plc., P.O. Box 100, H-1475 Budapest, Hungary

ARTICLE INFO

Article history:
Received 2 June 2009
Received in revised form 22 July 2009
Accepted 28 July 2009
Available online 4 August 2009

Keywords:
Raman spectroscopy
Chemical imaging
Tablet manufacturing
Tablet composition
Polymorphism

ABSTRACT

Raman imaging method was used to characterize the effect of different manufacturing technologies on properties of the produced tablets, such as compound distribution, polymorphism, strength, and estimated active pharmaceutical ingredient (API) content. The obtained chemical maps were evaluated based on their visual appearance and on the statistical properties of the component scores obtained by direct classical least squares (DCLS) modelling. It is demonstrated that changes in the distribution of the API and excipients can be detected with chemical imaging and these differences are in close relationship with the applied granulation method and with the mechanical properties of the analyzed tablet. It is also shown that the chemical images used for characterizing the component distribution can also be processed for obtaining a cautious estimation to the mass fractions of the components.

1. Introduction

The use of chemical imaging based on vibrational spectroscopy has been rapidly increasing in the past decade, especially in the pharmaceutical technology. Mostly IR, NIR and Raman microspectrometry have been used. Raman imaging combines the beneficial properties of Raman spectrometry, such as negligible sample preparation and sharp vibrational bands, with the power of high-resolution chemical imaging in detecting patterns and heterogeneity in the analyzed samples. The micro-spectrometric techniques apply two approaches, the global imaging and point mapping techniques, for characterizing an area. Both techniques provide a hypercube of data with two spatial and one spectral dimension. The point mapping configuration, usually used in Raman imaging, obtains the image by taking the spectrum of a single point (or a line of several points) and then stepping to another point, where the next spectrum is accumulated. A grid of these single points forms the spectral image of the sampled area. With this set-up one can control the spatial grid, thus the area and the spatial resolution of the images can be adjusted. All techniques used in chemical imaging are extensively described in Refs. [1,2].

In the field of vibrational chemical imaging several laboratories have used various chemometric methods to process the hyperspectral data. The most unambiguous way to visualize the distribution of components is, however, to collect the spectra of the pure components and model them with direct classical least squares (DCLS) method. Since the real components are being used, this allows to create the most accurate distribution maps [3,4], and DCLS also gives information, to a certain extent, about the relative concentrations of constituents [4].

The applications of chemical imaging are multiplying covering more and more fields within the pharmaceutical technology. Homogenization of powder blends is monitored mostly by NIR imaging [5–8]. Solid dispersions of drugs have been characterized by Raman microscopy [9–11], evaluating the degree of amorphization [9] or physicochemical stability [10]. Solid dispersions produced by extrusion were also analyzed and it was found that extrusion leads to homogeneous compound distribution [12]. Compound visualization was carried out in granules via NIR chemical mapping and Raman global imaging [13], while Raman line mapping was used to analyze multilayered particles [4].

Tablets are the pharmaceutical samples analyzed most frequently via Raman imaging. The questions to be answered with chemical imaging include visualization of the compound distribution [14–20], minor component detection [21], and determination of API content [18]. Chemical imaging and Raman spectrometry have also turned out to be a very effective method in identifying and characterizing counterfeit products [22–26].

In a few cases the authors extracted process-related information about the samples. NIR chemical imaging has been recently used to determine the distribution of density and tabletting force and to investigate the effect of the amount of lubricant added. Henson

* Corresponding author. Tel.: + 36 1 463 5918.
E-mail addresses: balazs.vajna@gmail.com, vajesz@gmail.com (B. Vajna).

0731-7085/$ – see front matter © 2009 Elsevier B.V. All rights reserved.
doi:10.1016/j.jpba.2009.07.030

Table 1
Composition of tablets.

Ingredient	Commercial name	Mass fractions
API (imipramine hydrochloride)	Imipramine HCl	10%
Microcrystalline cellulose (MCC)	Avicel PH102	76%
Maize starch	Sta-RX 1500	10%
Hydroxypropyl-methyl-cellulose (HMPC)	Pharmacoat 606	3%
Mg stearate (MgS)	Mg stearate	1%

and Zhang investigated the effect of the particle size distribution of the ingoing API material on the domain size of the API in the tablet [27]. There have also been some attempts to compare slight differences in certain manufacturing technologies via Raman imaging [2,17]. However, as far as the authors are aware, Raman chemical mapping has not yet been used to systematically analyze the effect of the production technology on the spatial distribution of the ingredients.

The aim of this study was to determine the spatial distribution of the API and other ingredients in tablets of the same composition but manufactured with different methods. This approach may help in understanding the differences in the drug release kinetics and mechanical behaviour of the tablets. Another aim was to test the reproducibility of semi-quantitative determination of the components and to find out whether the formulation technology has an effect on the estimation. Since it is crucial to explore the structure–property relationships of pharmaceutical products, the described aims represent an important step to the realization of the PAT (Process Analytical Technology) initiative [2]. Furthermore, the capability of distinguishing the different manufacturing technologies from each other makes the identification of counterfeit products easier.

2. Materials and methods

2.1. Materials and tablet preparation

The model tablets contained imipramine hydrochloride (provided by EGIS Pharmaceuticals Plc., Budapest, Hungary) as the active pharmaceutical ingredient. Further ingredients were microcrystalline cellulose (FMC BioPolymer, Princeton, USA), maize starch (Colorcon, West Point, USA), hydroxypropyl-methyl-cellulose (Shin-Etsu, Tokyo, Japan) as binder and magnesium stearate (Faci Spa, Carasco, Italy) as lubricant.

The composition and mass fractions (identical for all tablets) can be seen in Table 1. Seven different manufacturing methods were used, signed as D, HS-W, HS-A, F-W, F-H, F-A and F-AH (see Table 2). "D" tablets were produced without any granulating steps; all ingredients were directly compacted on a Fette EX1 eccentric press. In the cases of HS-W and HS-A batches the ingredients were aggregated via high-shear granulation method in a Pro-C-ept 4M8 high-shear granulator. In the HS-W case the API was mixed with the other ingredients in solid form, using pure water as granulating liquid. In the HS-A case only the inactive excipients were inserted into the vessel, and the API was solved beforehand in water, using this solution for granulating. After drying to 2% remaining moisture and homogenizing the granules with Mg stearate and a small remaining portion of cellulose, the mixture was compacted on the same device as mentioned before. In the F-W,H,A,AH batches the granulation was carried out in a Glatt GCPG-1 fluid bed granulator, with granulating liquid of pure water, HPMC solution, API solution and API-HPMC co-solution, respectively. The remaining ingredients were added in solid form, with extragranular addition of Mg stearate and some Avicel after the granulation and drying (to 2% moisture) were complete.

The same mixing time and blending rotor speed was used in all the batches. Tablets, of flat surfaces, were compressed with compaction forces of 5 kN, 10 kN and 15 kN.

2.2. Tablet analysis

After preparation the mechanical properties of tablets in each batch were tested. Since these pharmaceuticals were not produced for commercial use, the questions were focused only on the mass (for controlling the sample properties) and the tablet hardness. Tablet hardness analysis was carried out on a PharmaTest PTB-311 device, measuring 10 tablets of each compression force level in each batch.

2.3. Raman micro-spectrometry

Raman-mapping spectra were collected using a Horiba Jobin-Yvon LabRAM system coupled with an external 785 nm diode laser source and an Olympus BX-40 optical microscope. Objectives of 10× and 100× magnification were used for optical imaging and spectrum acquisition. The laser beam is directed through the objective, and backscattered radiation is collected with the same objective. The collected radiation is directed through a notch filter that removes the Rayleigh photons, then through a confocal hole and the entrance slit onto a grating monochromator (950 groove/mm) that disperses the light before it reaches the CCD detector. The spectrograph was set to provide a spectral range of 400–1630 cm^{-1} and 2 cm^{-1} resolution.

The Raman spectra of the ingredients were collected with a 100× objective using an acquisition time of 100 s and accumulating two measured spectra at a time. The reference spectra of each component were achieved by averaging five such spectra in order to increase signal to noise ratio, to decrease background deviation and to test the homogeneity of the used ingredients.

Raman-mapping was performed on the surface of the tablets. No sample preparation was applied in order to avoid alteration of the original sample structure. The low-resolution maps were collected with 10× objective (laser spot size: ~4 μm) and 10 μm step size, while 100× magnification (laser spot size: ~1 μm) and 2 μm step size were used when creating high-resolution images. Six additional low-resolution maps were taken from three tablets in the HS-W batch to determine within-tablet and among-tablets devia-

Table 2
Manufacturing methods.

Batch	Manufacturing method			
	Technology	Granulating liquid	Drying	Compaction force
D	Direct tabletting	–	–	5, 10 and 15 kN
HS-W	High-shear granulation	Water	Cabinet dryer	5, 10 and 15 kN
HS-A	High-shear granulation	10% API solution	Cabinet dryer	5, 10 and 15 kN
F-W	Fluid bed granulation	Water	Fluid bed	5, 10 and 15 kN
F-H	Fluid bed granulation	10% HPMC solution	Fluid bed	5, 10 and 15 kN
F-A	Fluid bed granulation	10% API solution	Fluid bed	5, 10 and 15 kN
F-AH	Fluid bed granulation	Solution containing 15% API and 4.5% HPMC	Fluid bed	5, 10 and 15 kN

tions. Four additional chemical images were recorded from the F-H batch to determine the effect of the measured area on the accuracy of the estimation of ingredient concentrations. Three tablets were analyzed in the D, HS-W, and F-W batches with 10× magnification and 100 μm step size to estimate tablet composition and to test the reproducibility of the method. (This set-up was used in order to ensure the independence of the adjacent pixels.) In each experiment the acquisition time of a single spectrum was 30 s and two spectra were averaged at a time. The measured area, when the 10× objective were used, varied from 28 × 28 to 34 × 34 pixels depending on the available measurement time. Maps recorded with the 100× objective consisted of 60 × 60 pixels.

2.4. Data analysis

The spectrum set of a mixture (containing k components) can be mathematically described, if the interactions between the constituents are negligible (which can be assumed in the case of pharmaceutical products), in the following way:

$$\boldsymbol{X} = \boldsymbol{C}\boldsymbol{S}^{\mathrm{T}} + \boldsymbol{E} \tag{1}$$

$\mathbf{S}^{\mathrm{T}}$ ($k \times \lambda$) is the set of reference (pure component) spectra, each spectrum consisting of λ intensity values and forming a row in the matrix. $\mathbf{X}$ ($p \times \lambda$) is the matrix containing the mapping spectra, and $\mathbf{C}$ ($p \times k$) contains the vectors of spectral concentrations (each row in $\mathbf{C}$ contains the concentrations of the k ingredients). The matrix $\mathbf{E}$ represents the residual noise. It should be noted that the data is originally acquired in a three-dimensional hypercube form ($n \times m \times \lambda$), thus, the data has to be unfolded into a two-dimensional matrix beforehand. One-way to do this is to unfold the spatial dimensions, acquiring the $\mathbf{X}$ matrix with $p = n \times m$ rows and λ columns. The alignment of the above mentioned matrices are visually illustrated in Ref. [1].

The images were obtained by DCLS modelling of the spectra of each analyzed point, using the spectra in Fig. 1 as reference ($\mathbf{X}$). The spectral concentrations are estimated by the following way [1]:

$$\boldsymbol{C} = \boldsymbol{X}\boldsymbol{S}(\boldsymbol{S}^{\mathrm{T}}\boldsymbol{S})^{-1} \tag{2}$$

Before applying the DCLS method, all spectra were baseline corrected. (This was done with the same baseline for all the maps and reference spectra.) The measured spectra were normalized to eliminate the intensity deviation between the measured points. DCLS was applied on the whole spectral range using Eq. (2). The obtained concentration-like parameters (the calculated c_{ij} values of the $\mathbf{C}$ matrix) were then re-scaled with Eq. (3) to give the estimated concentrations of the ingredients (c'_{ij} is the spectral concentration of component j in point i). The re-scaled spectral concentrations (Raman DCLS scores) are plotted against the X and Y spatial coordinates, producing a score map. A scale bar is given to the images, which shows the correlation between the colour of a pixel and the Raman DCLS score of the component in that particular pixel.

$$c'_{ij} = \frac{c_{ij}}{\sum_{j=1}^{k} c_{ij}} \tag{3}$$

The statistical properties, e.g. relative standard deviation (RSD) of the Raman scores of each point on a map provide further information about the differences between the batches. The RSD and the maximum observed value (MAX) were used. The RSD corresponds to the magnitude of differences among the points on a surface, while the maximum observed value shows the Raman score on the area with the thickest API layer or particle.

The mean and median values correspond to the overall API concentration, but since every tablet had the same composition, they were used to control the reproducibility of the mapping method and initially their differences were not directly correlated to the manufacturing technologies.

Univariate modelling was also applied to produce images in the case of each batch and these images were compared to the DCLS score maps. The latter images were less noisy and more suitable in every case, thus, the univariate images are not discussed in this paper.

All visualized score maps were created with LabSpec 5.41 (Horiba Jobin-Yvon) software, while statistical analyses were carried out with MATLAB 7.6 (MathWorks) and Statistica 8.0 (StatSoft).

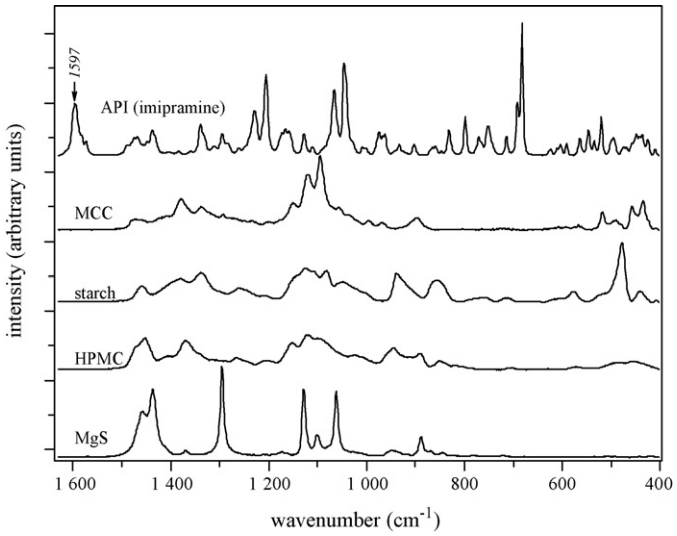

Fig. 1. Raman spectra of the pure ingredients.

3. Results and discussion

The first task of the analyses was to explore the differences in the compound distribution between tablets produced with different manufacturing technologies. Thus, distribution maps were created with low and high spatial resolution (compared to the average particle sizes of the ingredients), in order to determine the characteristics of each technology. Further experiments were carried out using the high-resolution set-up to find out if additional information can be obtained this way. Additionally, these maps were evaluated for obtaining complementary information such as polymorphism of the ingredients and an estimation of the composition. Tablets prepared with different compaction pressure levels were also tested to see if the created hyperspectral images contain information about the degree of compression.

3.1. Reference spectra

Reference Raman spectra of the pure components were accumulated for the DCLS modelling. The acquired spectra are shown in Fig. 1. The API band at 1597 cm^{-1} allows reliable determination of the API content with both univariate and DCLS modelling, since the other ingredients do not have an overlapping band in that spectral region.

3.2. Comparing low-resolution maps

In the pharmaceutical application of Raman-mapping it is beneficial to analyze as large area as possible. Thus, at first, maps were created with increased laser spot size (10× objective) and lower spatial resolution, enabling a larger sample surface to be investigated.

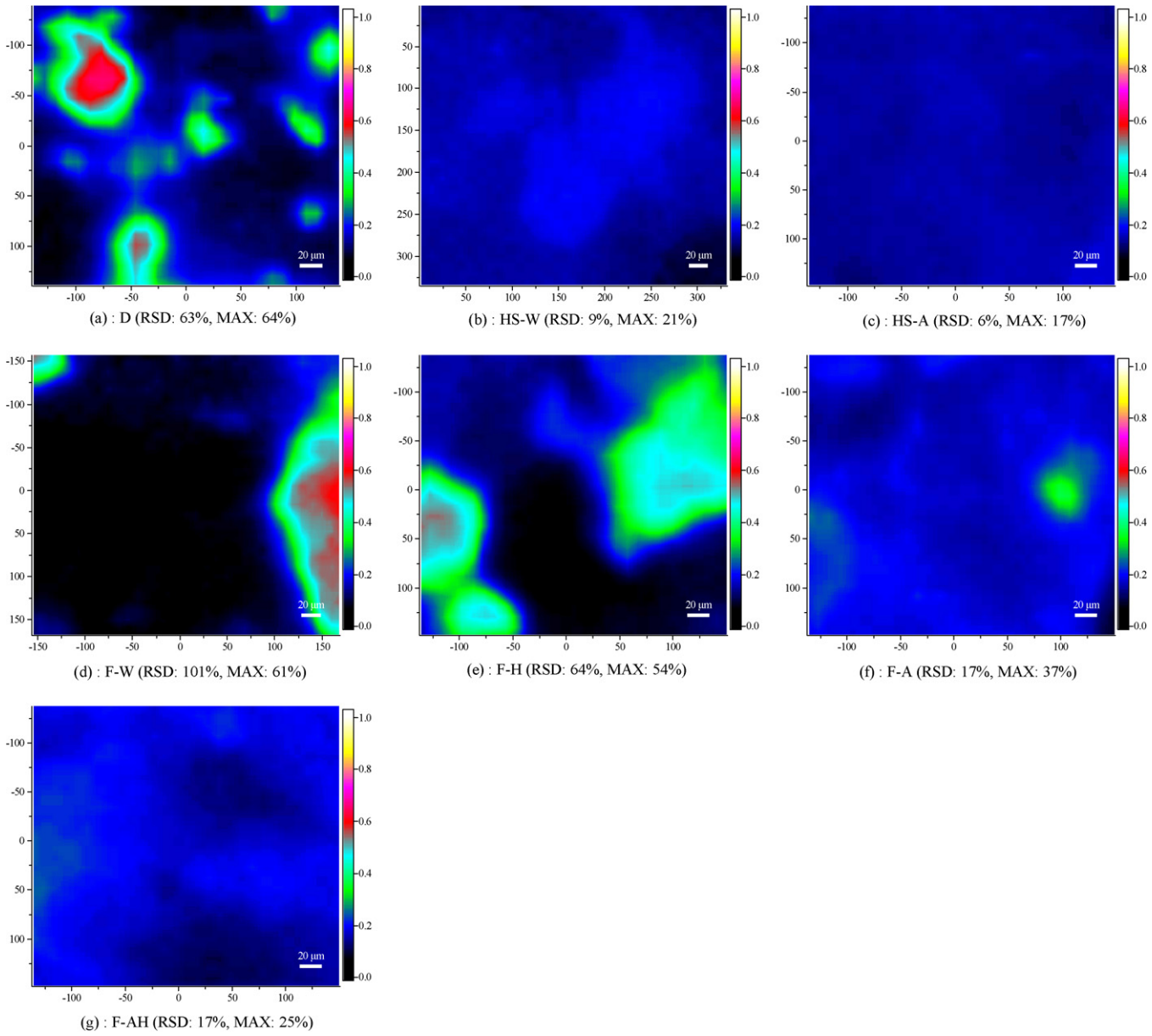

Fig. 2. Spatial distribution of API (in a completely black pixel the selected ingredient cannot be detected, while in a white pixel the Raman score is high according to the scale bar on the right side of each image). (a) D (RSD: 63%, MAX: 64%), (b) HS-W (RSD: 9%, MAX: 21%), (c) HS-A (RSD: 6%, MAX: 17%), (d) F-W (RSD: 101%, MAX: 61%), (e) F-H (RSD: 64%, MAX: 54%), (f) F-A (RSD: 17%, MAX: 37%), and (g) F-AH (RSD: 17%, MAX: 25%).

Fig. 2 compares the spatial distribution of the API in the batches of different technologies. In case of direct tabletting (batch D) the API exists in distinct particles, and it was not detected at all in certain areas. With an appropriately large sample surface the particle size distribution can be estimated (as reported in [28]). When applying high-shear granulation with water (HS-W), however, the API is distributed almost equally on the sampled area. On the other hand, slight differences occur in the layer thickness or the concentration of the API. High-shear granulation performed with the solution of the API (HS-A) leads to a perfectly homogenous API distribution in the sample.

The granulation phase of manufacturing is often performed in a fluidized bed, where the wetting and drying of fluidized particles take place simultaneously, giving shorter time for the API to start dissolving in the granulating liquid. This case can be seen in Fig. 2d and e. The API was added in powder form and the smaller particles got solved, while the large particles remained in original unsolved form. The layer thickness in the fluid granulation showed larger deviation than in the high-shear granulation, as shown in Fig. 2f and g, even if the drug was solved in water beforehand (alone or together with HPMC). This can be explained by the simultaneous wetting and drying of the particles, since the droplets of the granulating solution do not have enough time to form a homogeneous layer on the surface. This results in a surface with moderately heterogeneous API layer. (The same applies to the HPMC in the F-H and F-AH technologies.)

The values of relative standard deviation (RSD) and maximum observed score (MAX) also differ significantly among the batches of dry, high-shear and fluid technologies. RSD itself is enough to differentiate high-shear granulation from the other techniques (<9% in HS granulation, while >17% in any other batch, see Fig. 2). This is due to the fact that the API forms upon drying a homogeneous layer on the particles of the excipients, as the images (Fig. 2b and c) also imply. The low RSD value confirms the homo-

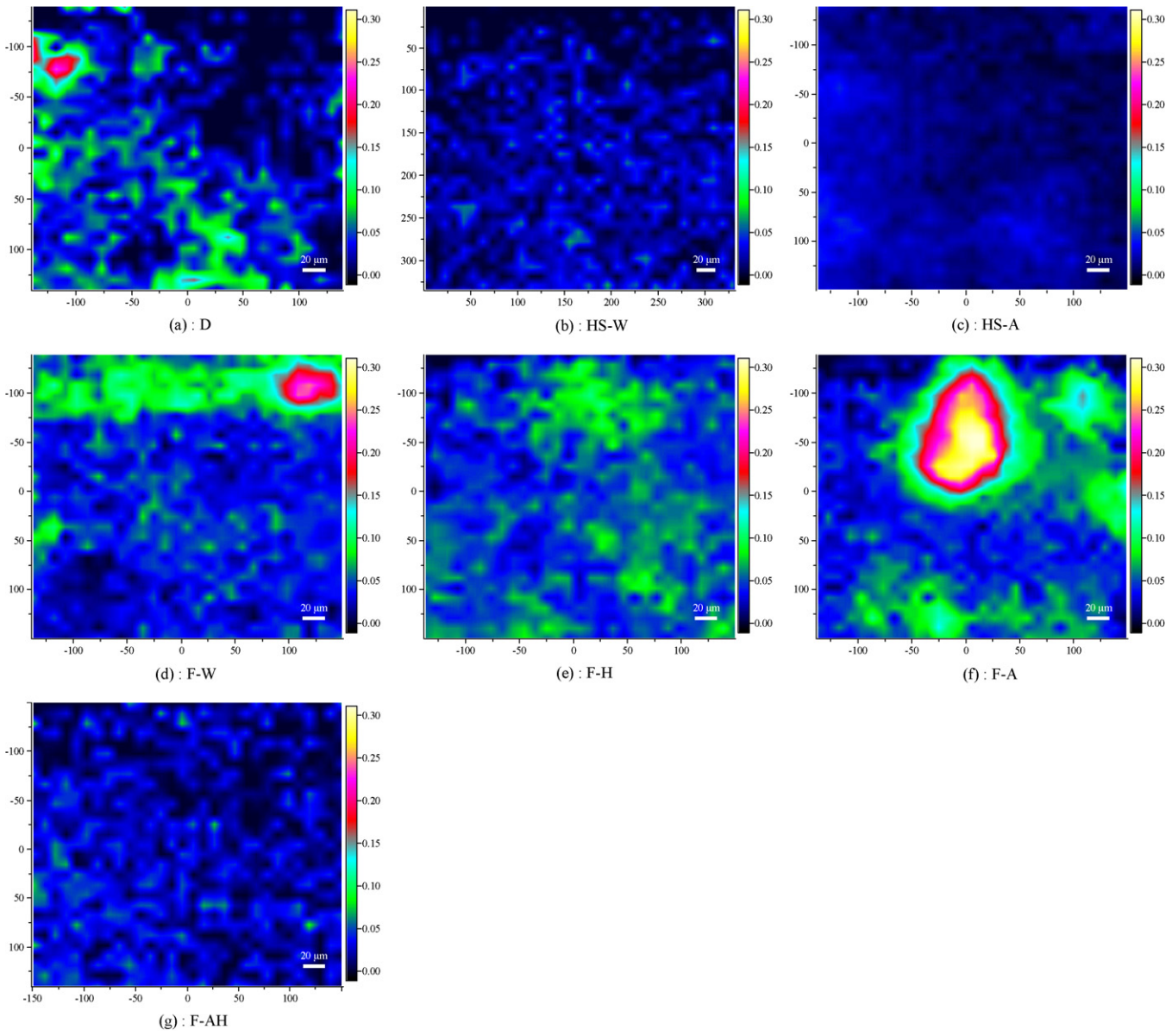

Fig. 3. Spatial distribution of HPMC (at a completely black pixel the selected ingredient cannot be detected, while at a white pixel the Raman score is 0.3 or higher according to the 0–0.3 image scale). (a) D, (b) HS-W, (c) HS-A, (d) F-W, (e) F-H, (f) F-A, and (g) F-AH.

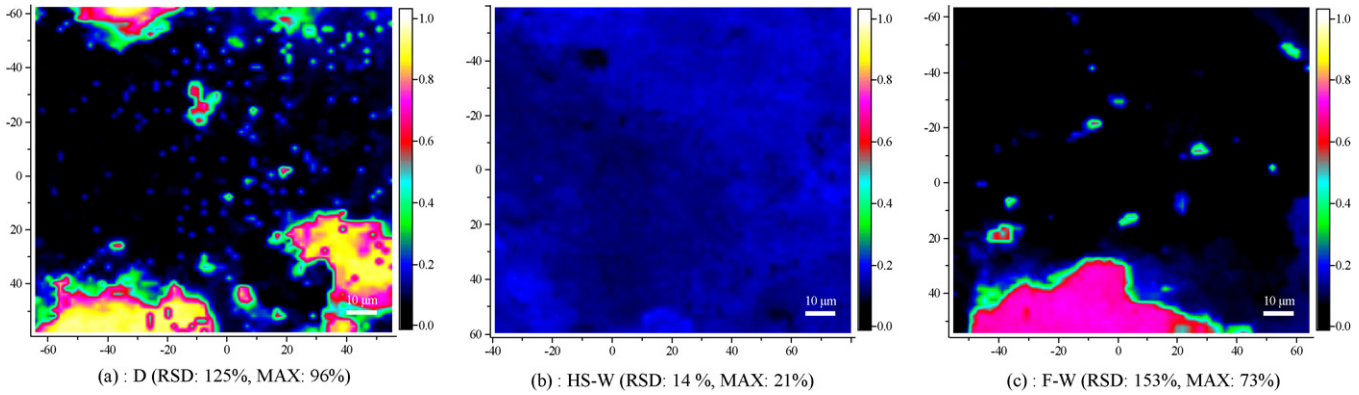

Fig. 4. Spatial distribution of imipramine using 100× magnification and 2 μm step size. (a) D (RSD: 125%, MAX: 96%), (b) HS-W (RSD: 14 %, MAX: 21%), and (c) F-W (RSD: 153%, MAX: 73%).

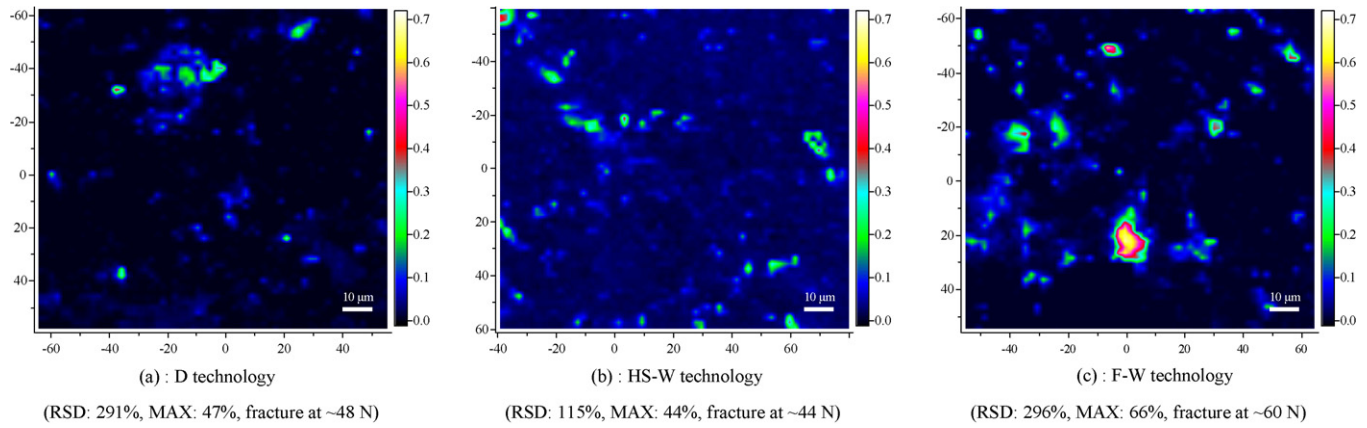

Fig. 5. Spatial distribution of Mg stearate using 100× magnification and 2 μm step size. (a) D technology (RSD: 291%, MAX: 47%, fracture at ~48 N), (b) HS-W technology (RSD: 115%, MAX: 44%, fracture at ~44 N), and (c) F-W technology (RSD: 296%, MAX: 66%, fracture at ~60 N).

geneous distribution. The difference between the HS-W and HS-A batches also appears in the numbers: the slight inhomogeneity of the layer thickness in HS-W results in a higher RSD of the API Raman score. This shows that completely equal distribution could only be acquired if the API was first solved in water and then added to the excipients.

In contrast, to distinguish the dry compaction from the fluid technology, both the RSD and MAX values are required. The images show that the main difference between the direct tabletting and the F-W fluid method (where the solid drug is introduced to the fluid bed) is that the water solves the smaller particles, while the large particles remain unaffected. As a result, in the F-W case, one can find mostly very low or relatively high values, which results in a much higher RSD (101%) than in the D tablet (64%). On the other hand, the MAX score is somewhat lower in the case of F-W (61%) than in D (64%). The lower peak score refers to lower particle thickness in the *Z* dimension, proving that even the larger API particles are partially solved in the granulating liquid during the manufacturing process. This effect can also be seen in the F-H case (where the peak score is 54%). However, the RSD was found to be much lower than in F-W (64%). In the F-A and F-AH batches, the RSD and MAX values of the API Raman score are very close, since the API was solved in the granulating liquid in both cases.

Maps with 100 μm step size (where the adjacent pixels are almost totally independent from one another) showed the same trends in the distribution of the components and in the statistical properties (RSD and MAX) as those given above.

Based on the described results one can conclude that investigating only one component is not enough to distinguish between the F-W, F-H and the F-A, F-AH technologies. However, analyzing the distribution maps of each component reveals that the differences in the preparation method appear in the distribution of not only the API, but also the HPMC.

Fig. 3 shows the spatial distribution of HPMC in each batch. (The statistical data of HPMC Raman scores are not given due to the small concentration and thus stronger modelling error.) The images prove that while HPMC is properly solved and well distributed during the high-shear granulation process, the fast drying in the fluid bed leaves too short time for the HPMC particles to be solved. Homogeneous HPMC distribution can be achieved if it is solved in water and this solution is used as the granulation liquid. In conclusion, more details can be explored about a technology (in this case all the technologies could be distinguished) if one investigates the distribution of all the ingredients. As seen in Fig. 3, even minor components (such as HPMC) can be analyzed this way, however, the evaluation of the distribution of the lubricant required maps created with higher magnification.

These results show that low-resolution maps provide information about a relatively large area on the investigated sample. However, higher resolution analysis is also needed to explore the small-scale details of the distribution of the API and to visualize the distribution of components of very low concentration and small particle size.

3.3. Comparing high-resolution maps

The detailed image of the dry technology batch reveals that small (<3 μm diameter) particles can be found on the tablet surface. Mapping of API (Fig. 4a) indicated that the relevant pixels have significantly higher API concentration than the pixels nearby. Such small particles are characteristic to the dry technology. In the tablets of fluid bed granulation (F-W, for example), mainly larger particles could be detected (the appearance of 1-pixel sized particles is exceptional). Regarding the high-shear technology, the distribution of components is generally homogeneous, but minor local inhomogeneities were found too. This proves that the granulation time was not long enough to dissolve the API completely.

Using high spatial and optical resolution the distribution of minor components – such as Mg stearate – can also be visualized. The laser spot size and the sampled depth with the 10× objective is too large to capture a Mg stearate particle. With 100× magnification, however, distinct particles of the lubricant can be detected. As shown in Fig. 5, we experienced significant difference in the lubricant homogeneity between the HS-W and the F-W batches. In the F-W batch the lubricant is present in distinct particles, and cannot be detected in the other points, while in the HS-W tablets the lubricant was detected all over the sample.

These results indicate that minor ingredients can also be investigated with chemical imaging, which can be used for understanding differences in macroscopic (e.g. mechanical) properties.

The results of the tablet hardness measurements are shown in Table 3. These make clear that the fracture of D and F-W tablets occur at higher forces than in case of the HS-W tablets, no matter the compaction force used in the manufacturing process. It is

Table 3
Tablet hardness test of each batch (the values are averages of 10 tablets and their confidence intervals at 95% confidence level).

Compaction force	Tablet hardness (fracture force)		
	Batch D	Batch HS-W	Batch F-W
5 kN	27.2 N (±0.9 N)	24.4 N (±0.3 N)	31.3 N (±0.5 N)
10 kN	48.4 N (±1.1 N)	43.8 N (±0.7 N)	60.1 N (±1.4 N)
15 kN	65.4 N (±1.6 N)	52.6 N (±1.4 N)	59.9 N (±1.1 N)

clear from Fig. 5 that the well-dispersed lubricant in the case of HS-W process decreases the cohesion among the particles causing lower tablet strength than those of other processes. The difference between D and F-W processes can be explained by the smaller particles detected in case of D sample (Fig. 4a), which require higher compaction force to achieve high strength.

3.4. Effect of technology on polymorphism

The manufacturing technology often influences the polymorphism. The changes in the morphology may also help to determine the technology used for production. The presence of moisture in course of the process, for instance, can change the morphology of the API as it happened in the case shown in Fig. 6.

It can be seen that if the ingredients are compressed directly, without any wet granulation step, the spectrum of the imipramine particles shows no change compared to the original API. However, significant changes can be observed when the API gets in contact with moisture. There is a band system with overlapped peaks at 975 cm^{-1}, 967 cm^{-1} and 962 cm^{-1}. After wetting and drying the band at 967 cm^{-1} gets stronger than the other two, and the band at 497 cm^{-1} becomes strong as well. The band system originally at 450 cm^{-1} and 436 cm^{-1} also suffers change, but the most significant alteration is the concurrent widening of the band at 684 cm^{-1} and disappearance of the peak at 692 cm^{-1}. Since neither of the new bands can be related to the other ingredients, these phenomena are the consequences of morphological change of the API during the processing.

3.5. Correlation of compaction force and Raman spectra intensity

Besides the discussed pre-tabletting steps the correlation between the compaction force and Raman intensity was also investigated. Further Raman maps were accumulated from the raw granule set and from tablets pressed with 5 kN, 10 kN and 15 kN to determine the effect compaction force on the Raman spectra and the component distribution. For the preliminary analysis, the 100× objective was used. We found that the compound distribution does not depend on the compaction circumstances; however, the overall Raman intensity shows clear correlation with the applied force level. This can be easily understood considering the fact that higher tabletting pressure results in more compact substance and less trapped air inside the tablets. The increased concentration of the ingredients in the sampled volume leads to increased peak intensities. It must be emphasized that in this study a large number of spectra (~1000) were acquired from each tablet to achieve good correlation between the overall Raman intensity of the map spectra and the used compaction force (Fig. 7).

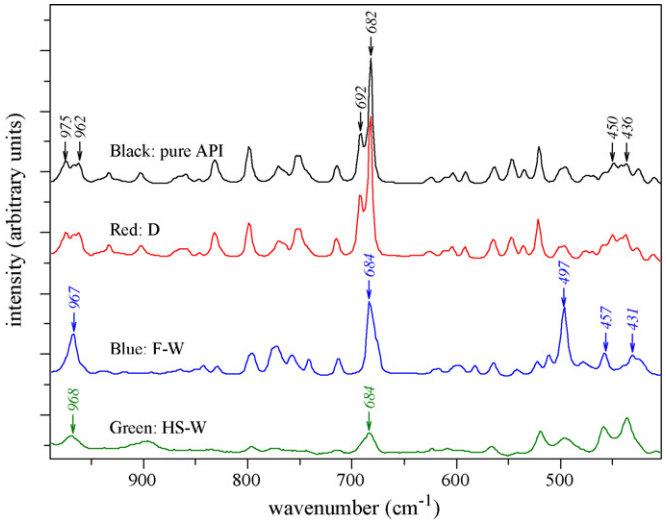

Fig. 6. Spectra of API in pure form and in different tablets. DCLS-modelled API score is 96% in the D, 84% in the F-W and 23% in the HS-W spectrum.

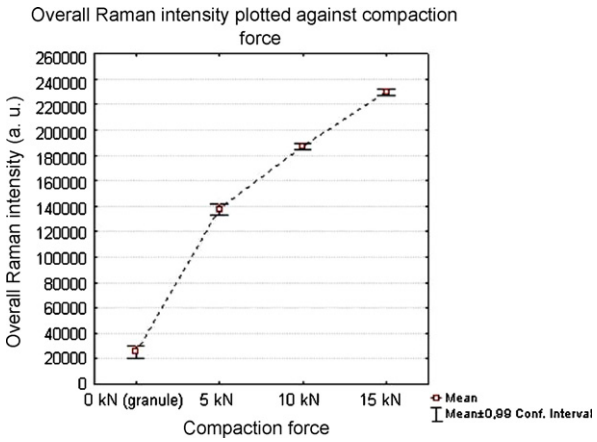

Fig. 7. Overall Raman spectrum intensity plotted against the applied compaction force.

3.6. Estimation of the composition of tablets

The DCLS scores of an ingredient are in correlation with the real concentration. A quantitative in-depth analysis requires calibration, which is a very lingering procedure if a system contains a large number of ingredients. Beyond the visualized chemical images, shown in the previous sections, it was also challenging whether the chemical images contain reliable semi-quantitative information about the composition of a tablet. Since a semi-quantitative analysis requires the independence of the adjacent pixels, the step sizes in these maps were increased to exceed the average particle size of the ingredients. The maps introduced in Section 3.2 (10× magnification, 10 μm step size) were also considered for comparison.

The mean and median values of the API scores on a map were tested, along with the API score in the modelled average spectrum of a map, and these were compared to the real tablet composition (given in mass fractions). It was found that modelling of the spectra followed by averaging their Raman scores provides the same results as the process when the spectra are averaged first and then the mean spectrum is modelled with Eq. (2). The difference between the obtained tablet compositions with the two methods did not exceed the value of 0.8% in any case. Since modelling the mean spectrum is a much faster and more straightforward method, this was used in all further calculations. It should be noted hereby that the correlation between the Raman scores and the true composition is not properly defined, thus these results serve only a semi-quantitative approach.

Table 4
Composition of tablets according to the Raman CLS scores, after correction.

Ingredient	Batch D[a]	Batch HS-W[a]	Batch F-W[a]	Batch F-H[b]	Real composition (mass%)
API	10	10	10	10	10.0
MCC	67.4	71.0	70.6	70.4	76.0
Starch	15.6	10.5	10.7	12.3	10.0
HPMC	5.5	6.0	7.4	5.9	3.0
MgS	1.4	2.5	1.3	1.4	1.0

[a] Contains maps with 100 μm spatial resolution.
[b] Contains maps with 10 μm spatial resolution.

Table 5
Reproducibility of maps collected from HS-W tablets.

	Map no.										Mean	SD
	1[a]	2[a]	3[a]	4[a, c]	5[a, c]	6[a, c]	7[a,c]	8[b]	9[b]	10[b]		
Number of pixels	1089 33 × 33	1089 33 × 33	841 29 × 29	961 31 × 31	1023 31 × 33	1156 34 × 34	841 29 × 29	900 30 × 30	1089 33 × 33	900 30 × 30	Sum: 9889	–
API mean score	15.9	15.5	15.3	16.9	16.2	16.5	16.8	15.8	16.1	15.5	16.0	0.52

[a] Maps with 10 μm step size.
[b] Maps with 100 μm step size.
[c] Maps acquired from the same tablet (within-tablet reproducibility).

The scores calculated from the maps exhibit moderate deviation that can be ascribed mainly to the differences in the manufacturing technology. The estimated API content in batch D is significantly higher than that of the other batches. This implies that the manufacturing technology is advisable to be determined before the assessment of the composition is started. The obtained Raman scores (keeping in mind that they are not concentrations themselves) are numerically not far from the real tablet composition. These approximate values may be helpful in the analysis of tablets of unknown composition. (The DCLS modelling requires the knowledge of the spectra of ingredients, though.) In addition, considering the fact that the dosage of the drug is generally known from independent analysis or information, an empirical correction may be applied to re-scale the score percentage of the other excipients. For example, in the system discussed above, the tablets contain 10% imipramine, so the empirical API score shall also be set to 10%. All remaining (or missing) score points are distributed among the other ingredients keeping their original relative percentage ratio. The corrected scores provide estimation for the tablet composition (Table 4).

The alterations from the real composition can be interpreted based on the characteristics of each process, which needs, however, further consideration.

The reproducibility tests (introduced in the beginning of Section 3) showed that increasing the step size from 10 μm to 100 μm between the adjacent measured points decreases the deviation among the estimated composition of the tablets. This is due to the fact that if the step size exceeds the sizes of the particles, the adjacent points become independent from each other, which leads to more reliable results. It was also found that, not surprisingly, maps with larger number of pixels show smaller deviation in the average component scores. Evaluation of the 10 maps acquired from HS-W tablets made possible to compare the within-tablet and the within-batch reproducibility. As seen in Table 5, maps 4–7 were acquired from the same tablet and all of them showed higher API mean score than the maps taken from the other tablets (no. 1–3 and 8–10). This implies that this particular tablet had a somewhat higher API content than the other measured tablets. As a result, it can be presumed that the observed variance in the mean scores is partly due to the variance in the real composition of the tablets.

4. Conclusions

This study demonstrates the applicability of Raman-mapping in understanding the differences in the spatial distribution of constituents in differently manufactured tablets. Tablets with the same composition were prepared with seven distinct methods (including direct tabletting and several variations of high-shear and fluid granulation) and were analyzed via point-to-point Raman-mapping on the tablet surface. Based on the obtained chemical images all the batches of different technologies could be distinguished from each other (while multiple images of tablets from the same batch revealed the same distribution). This technique allows analysis and comparison of the main attributes of these batches, which may be useful for selecting the appropriate manufacturing technology. Using the 100× objective revealed further details about the spatial distribution of the components, and helps in the correct determination of the method of preparation and in the understanding of certain mechanical properties such as tablet hardness.

Besides the compound distribution, the hyperspectral images show that polymorphism of the API is also influenced by the different types of granulation methods. The Raman signals on a map can also be correlated to the applied compaction force during the tablet preparation.

Another outcome of this study is the application of Raman-mapping for the determination of the composition of ingredients in a tablet. It was found that modelling the spectrum of each pixel and averaging the DCLS scores give the same estimated composition as when the spectra of an image are averaged first and the mean spectrum is modelled with DCLS. In addition, the mean DCLS scores are numerically close to the real mass fractions; however, the manufacturing method also influences the estimated composition. Although the DCLS score of a component is not equivalent with the corresponding concentration level, it is demonstrated that the composition of a tablet can be cautiously estimated by simply considering the Raman DCLS scores and the dosage of the tablet. It is important to keep in mind that this is not a quantitative method, only a way to approximately guess the relative quantity of the ingredients in the pharmaceuticals.

The reproducibility of the method was also tested, and it was found that the visual characteristics and the statistical properties of the compound distribution maps were reproducible in all the tested batches. The mean values (the estimated composition) show moderate variation which can be reduced by increasing the number of analyzed points, or by increasing the step sizes among the pixels. In conclusion, micro-Raman spectrometry was found to be a reproducible and useful tool in the PAT initiative, since it makes possible to understand numerous distinct properties of tablets made with different manufacturing methods.

Acknowledgements

The authors would like to thank Mónika Agyagos in EGIS Pharmaceuticals Plc. for her help in the preparation of tablets. Dr. Pál Szepesváry is thanked for discussions regarding the evaluation of spectral matrices.

References

[1] C. Gendrin, Y. Roggo, C. Collet, Pharmaceutical applications of vibrational chemical imaging and chemometrics: a review, J. Pharm. Biomed. Anal. 48 (2008) 533–553.
[2] A.A. Gowen, C.P. O'Donnell, P.J. Cullen, S.E.J. Bell, Recent applications of Chemical Imaging to pharmaceutical process monitoring and quality control, Eur. J. Pharm. Biopharm. 69 (2008) 10–12.
[3] P.J. Treado, M.P. Nelson, Raman imaging, in: J.M. Chalmers, P.R. Griffiths (Eds.), Handbook of Vibrational Spectroscopy, vol. 2, John Wiley & Sons, London, 2002, pp. 1429–1459.
[4] S. Šašic, D.A. Clark, J.C. Mitchell, M.J. Snowden, A comparison of Raman chemical images produced by univariate and multivariate data processing—a simula-

tion with an example from pharmaceutical practice, Analyst 129 (2004) 1001–1007.
[5] A. El-Hagrasy, H.R. Morris, F. D'Amico, R.A. Lodder, J.K. Drennen, Near-infrared spectroscopy and imaging for the monitoring of powder blend homogeneity, J. Pharm. Sci. 90 (2001) 1298–1307.
[6] R.C. Lyon, D.S. Lester, E.N. Lewis, E. Lee, L.X. Yu, E.H. Jefferson, A.S. Hussain, Near-infrared spectral imaging for quality assurance of pharmaceutical products: analysis of tablets to assess powder blend homogeneity, AAPS PharmSciTech 3 (2002) 1–17.
[7] S.S. Sekulic, H.W. Ward, D.R. Brannegan, E.D. Stanley, C.L. Evans, S.T. Sciavolino, P.A. Hailey, P.K. Aldridge, On-line monitoring of powder blend homogeneity by near-infrared spectroscopy, Anal. Chem. 68 (1996) 509–513.
[8] E.N. Lewis, L.H. Kidder, E. Lee, NIR chemical imaging as a process analytical tool, Innov. Pharm. Technol. (2005) 107–111.
[9] N. Furuyama, S. Hasegawa, T. Hamaura, S. Yada, H. Nakagami, E. Yonemochi, K. Terada, Evaluation of solid dispersions on a molecular level by the Raman mapping technique, Int. J. Pharm. 361 (2008) 12–18.
[10] A. Docoslis, K.L. Huszarik, G.Z. Papageorgiou, D. Bikiaris, A. Stergiou, E. Georgarakis, Characterization of the distribution, polymorphism, and stability of nimodipine in its solid dispersions in polyethylene glycol by micro-Raman spectroscopy and powder X-ray diffraction, AAPS J. 9 (2007) E361–E370.
[11] E. Karavas, M. Georgarakis, A. Docoslis, D. Bikiaris, S.E.M. Combining, TEM, and micro-Raman techniques to differentiate between the amorphous molecular level dispersions and nanodispersions of a poorly water-soluble drug within a polymer matrix, Int. J. Pharm. 340 (2007) 76–83.
[12] J. Breitenbach, W. Schrof, J. Neumann, Confocal Raman-spectroscopy: analytical approach to solid dispersions and mapping of drugs, Pharm. Res. 16 (1999) 1109–1113.
[13] S. Šašic, Chemical imaging of pharmaceutical granules by Raman global illumination and near-infrared mapping platforms, Anal. Chim. Acta 611 (2008) 73–79.
[14] D. Clark, S. Šašic, Chemical images: technical approaches and issues, Cytometry 69 (2006) 815–824.
[15] C.T. Zugates, P.J. Treado, Raman chemical imaging of pharmaceutical content uniformity, Int. J. Vib. Spectrosc. (1999).
[16] L. Zhang, M.J. Henson, S.S. Sekulic, Multivariate data analysis for Raman imaging of a model pharmaceutical tablet, Anal. Chim. Acta 545 (2005) 262–278.
[17] S. Šašic, An in-depth analysis of Raman and near-infrared chemical images of common pharmaceutical tablets, Appl. Spectrosc. 61 (2007) 239–250.
[18] A. De Juan, R. Tauler, Spectroscopic imaging and chemometrics: a powerful combination for global and local sample analysis, Trends Anal. Chem. 23 (2004) 70–79.
[19] S. Šašic, M. Morimoto, M. Otsuka, Y. Ozaki, Two-dimensional correlation spectroscopy as a tool for analyzing vibrational images, Vib. Spectrosc. 37 (2005) 217–224.
[20] S. Šašic, D.A. Clark, J.C. Mitchell, M.J. Snowden, Analyzing Raman maps of pharmaceutical products by sample–sample two-dimensional correlation, Appl. Spectrosc. 59 (2005) 630–638.
[21] E. Widjaja, R. Kim, H. Seah, Application of Raman microscopy and band-target entropy minimization to identify minor components in model pharmaceutical tablets, J. Pharm. Biomed. Anal. 46 (2008) 274–281.
[22] S.E.J. Bell, J.R. Beattie, J.J. McGarvey, K.L. Peters, N.M.S. Sirimuthu, S.J. Speers, Development of sampling methods for Raman analysis of solid dosage forms of therapeutic and illicit drugs, J. Raman Spectrosc. 35 (2004) 409–417.
[23] S.E.J. Bell, L.J. Barrett, D.T. Burns, A.C. Dennis, S.J. Speers, Tracking the distribution of "ecstasy" tablets by Raman composition profiling: a large scale feasibility study, Analyst 128 (2003) 1331–1335.
[24] S.E.J. Bell, D.T. Burns, A.C. Dennis, J.S. Speers, Rapid analysis of ecstasy and related phenethylamines in seized tablets by Raman spectroscopy, Analyst 125 (2000) 541–544.
[25] S.E.J. Bell, D.T. Burns, A.C. Dennis, L.J. Matchett, J.S. Speers, Composition profiling of seized ecstasy tablets by Raman spectroscopy, Analyst 125 (2000) 1811–1815.
[26] P. de Peinder, M.J. Vredenbregt, T. Visser, D. de Kaste, Detection of Lipitor® counterfeits: a comparison of NIR and Raman spectroscopy in combination with chemometrics, J. Pharm. Biomed. Anal. 47 (2008) 688–694.
[27] M. Henson, L. Zhang, Drug characterization in low dosage pharmaceutical tablets using Raman microscopic mapping, Appl. Spectrosc. 60 (2006) 1247–1255.
[28] W. Doub, W. Adams, J. Spencer, L. Buhse, M. Nelson, P. Treado, Raman chemical imaging for ingredient-specific particle size characterization of aqueous suspension nasal spray formulations: a progress report, Pharm. Res. 24 (2007) 934–945.